Int J Adv Manuf Technol (2013) 66:1467–1473
DOI 10.1007/s00170-012-4431-6

ORIGINAL ARTICLE

Microstructure and mechanical properties of laser-MIG hybrid welding of 1420 Al-Li alloy

Jun Yan · Ming Gao · Geng Li · Chen Zhang · Xiaoyan Zeng · Ming Jiang

Received: 1 May 2012 / Accepted: 29 July 2012 / Published online: 12 August 2012

Abstract This paper investigates the microstructure and mechanical properties of 1420 aluminum–lithium (Al-Li) alloy joints before and after heat treatment by CO_2 laser-metal inter gas (MIG) hybrid welding. The 5-mm-thick 1420 Al-Li alloy plates were welded by CO_2 laser-MIG hybrid welding. Full penetration joints without any defects were produced. Optic and scanning electron microscopy were used to study the microstructure and fractograph characteristics. The results show that the microstructures of the heat-affected zone (HAZ) and fusion zone exist as a predominantly discontinuous equiaxed dendritic structure and as a fine cellular dendritic structure, respectively. After heat treatment, the microstructures change from dendritic structure to a spheroidal crystal; the grain size of fusion zone is obviously larger than that of the base metal and the HAZ. Furthermore, the hardness recovers substantially to a level similar to that of the parent material. The tensile strengths of the joints in the as-welded condition and after heat treatment are 223 and 267 MPa, reaching up to 57 and 68 % of the parent materials' strength, respectively. The fractographs show that the joint as-welded condition exhibits the characteristics of dominated dimples and a small amount tear ridges, which are associated with the mixed ductile and brittle facture mechanisms. The fracture mode transforms from a transgranular to an intergranular after heat treatment; cleavage cracking coupled with an intergranular microvoid coalescence fracture mechanism occurs.

Keywords Laser welding · Hybrid welding · Aluminum alloy

J. Yan · M. Gao · G. Li · C. Zhang · X. Zeng · M. Jiang
Wuhan National Laboratory for Optoelectronics,
College of Optoelectronic Science and Engineering,
Huazhong University of Science and Technology,
Wuhan, Hubei 430074, People's Republic of China

M. Gao (✉)
Division of Laser Science and Technology,
Wuhan National Laboratory for Optoelectronics,
Huazhong University of Science and Technology,
Wuhan, Hubei 430074, People's Republic of China
e-mail: mgao@mail.hust.edu.cn

1 Introduction

Aluminum–lithium (Al-Li) alloy has been widely employed in the aerospace industry for its excellent comprehensive properties, such as lower density, higher elastic modulus, and specific strength compared with traditional aluminum alloys. The joining techniques used in aircraft are mechanical fastening, which has the drawbacks of slow assembly and limitations in joining thin sections. To extend the range of applications and improve the overall performance, new joining methods are being developed.

Pickens have discussed the weld ability of Al-Li alloys in detail in a review [1]. The investigations about the Al-Li alloy by friction stir welding (FSW), laser welding, electron beam welding, and traditional arc welding had been reported widely. Madhusudhan investigated the 1441 Al-Li alloy by continuous current, pulsed current, and arc oscillation tungsten inert gas (TIG) welding. Microstructure refinement was observed in the case of pulsed current and arc oscillation TIG welding [2]. Chen and Huang studied the influence of welding parameters on the microstructures and mechanical properties of electron beam-welded 8090 Al-Li alloy plates [3]. Wei et al. and Shi et al. carried out a study on 1420 Al-Li alloy by FSW and laser welding, respectively [4, 5]. However, some difficulties are encountered in welding Al-Li alloy through these methods. For instance, vaporization of the low boiling point alloying element (Li and Mg) leads to some troubles in laser welding, whereas pores readily occur during electron beam welding. Arc welding is often sensitive to the formation of coarse grains in the heat-affected zone (HAZ), which

deteriorates the mechanical properties of the joints. Furthermore, as an alternative to weld aluminum alloy, FSW overcomes the problem of hot cracks; however, it also results in some problems by the softening of the welding nugget zone, thermal mechanical affected zone, and low welding speed [6–11].

As a new fusion welding method, the laser-metal inter gas (MIG) arc hybrid welding integrates laser beam and electric arc. The advantages of the hybrid process over arc welding and laser welding include higher welding stability, higher melting efficiency, easier addition of welding wires, and lower power input under the same penetration [12]. The hybrid welding method can overcome the disadvantage of alloy element vaporization, undercut, and high laser reflectivity in laser beam welding and remarkably improve the welding speed over arc welding. The investigations about laser-MIG hybrid welding steel have been reported widely and applied successfully in the industry. Zhang et al. examined the microstructure of AA6061 aluminum alloys using ER4043 filler wire by 4 kW Nd:YAG laser-MIG hybrid welding [13]. Kim et al. studied the welding phenomenon in AA 5083 butt joints with different gap conditions by laser-MIG hybrid welding [14]. Furthermore, some studies explored the effects of shielding gas, laser beam diameter, and process stability on the tolerance of joint gap and bead shape in laser-MIG hybrid welding [15–17]. However, few reports on Al-Li alloy welded by newly developed laser-MIG hybrid welding are available. Hence, the joint microstructure and mechanical properties of 1420 Al-Li alloys by CO_2 laser-MIG hybrid welding need further investigation.

In this study, the 5-mm-thick 1420 Al-Li alloy plates were welded by CO_2 laser-MIG hybrid welding. The joints were treated with solution heat treatment and artificial aging. The characteristics of macrostructure, microstructure, mechanical properties, and the microhardness of the joints were examined. Finally, the fractographs of weld joints were observed using a scanning electron microscope (SEM).

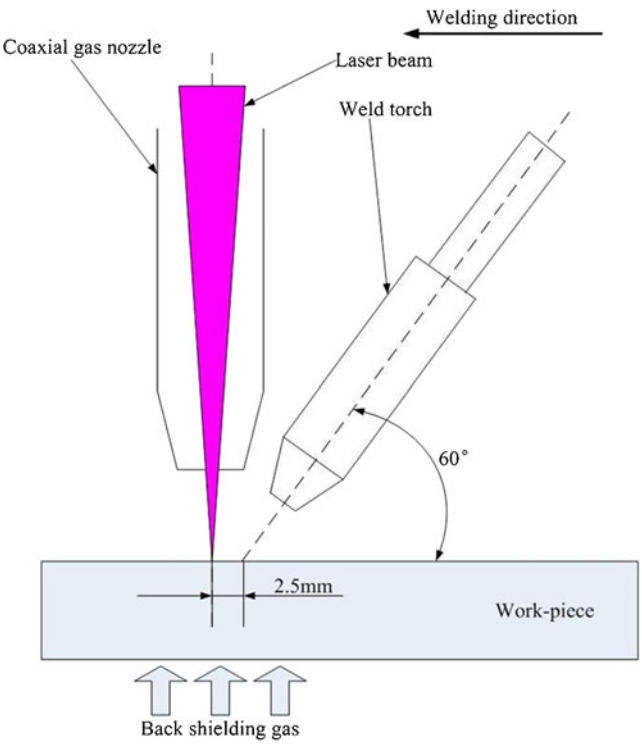

Fig. 1 Schematic diagram of CO_2 laser-MIG hybrid welding

Table 1 Chemical composition of parent material and welding wires, wt%

Composition	Li	Cu	Mg	Fe	Si	Al
Parent material	1.9–2.2	–	4.8–5.2	0.1	0.2	Remain
ER2319	–	5.8–6.8	0.02	0.3	0.2	

2 Experimental procedures

The laser-MIG hybrid system is composed of a CO_2 laser (Rofin TR050; maximum output power, 5 kW) and a MIG welder (Panasonic conventional DCEP; maximum output current, 350 A). This system is schematically shown in Fig. 1. The 5-mm-thick 1420 aluminum alloy plates and commercial ER2319 welding wires were used in the experiments. The nominal chemical composition of the substrate and the welding wires are listed in Table 1. The surface of the plates was cleaned, degreased, and dried before welding. The edges adjacent to the joints were mechanically prepared to minimize porosity. In the experiments, pure argon was used as the

Table 2 Experimental setup and parameters

Welding parameters	Value
Beam wave length (um)	10.6
Focus spot diameter (mm)	0.6
Focal length of lens (mm)	300
Unfocused length (mm)	−2
Wire extension length (mm)	14
Wire diameter (mm)	1.6
Coaxial gas nozzle pure He($L \cdot min^{-1}$)	7.5
MIG torch nozzle pure Ar ($L \cdot min^{-1}$)	15
Welding current (A)	75
Welding voltage (V)	16
Welding rate ($m \cdot min^{-1}$)	0.6
Laser power (kW)	2.0

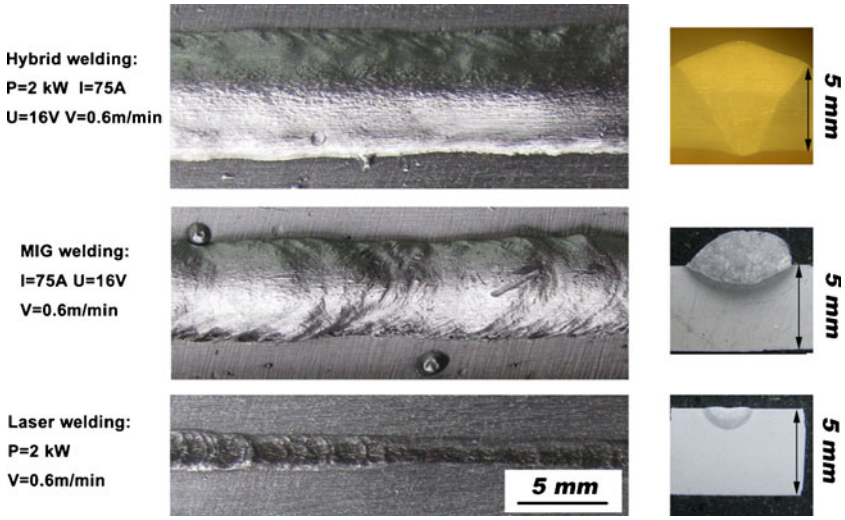

Fig. 2 Macrostructure of joints by laser, MIG, and laser-MIG hybrid welding

shielding gas for the back surface during welding. For the topside shielding, pure argon was provided by the MIG torch nozzle, and pure helium by the coaxial gas nozzle. The optimal welding parameters were chosen to achieve full penetration. The welding parameters are listed in Table 2 in detail. Cross-sections from the welded joint were prepared for optical microscopy examination using standard metallographic procedures. The mechanically ground and finish polished samples were etched using Keller's reagent. For the microhardness testing, a load of 200 g was used throughout the tests.

For post-welding solution heat treatment, weld samples were immersed in a salt bath at 460 °C for 20 min and then immediately quenched in air to room temperature. For the artificial aging treatment, the work pieces were placed in an oil oven at 120 °C, and the aging time was 10 h. To study the mechanical properties, the joints before and after heat treatment were sliced by abrasive cutters and then machined into the required dimensions to obtain tensile specimens. The fractured morphology of the specimens was analyzed through SEM.

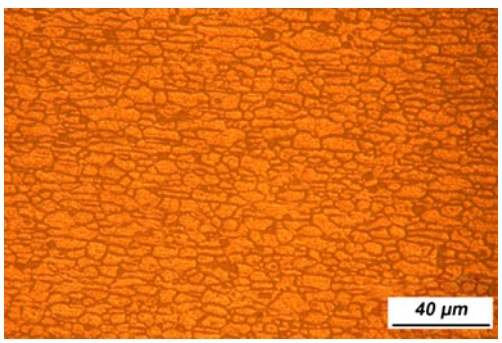

Fig. 3 Microstructure of 1420 aluminum alloy

3 Results and discussion

3.1 Macrostructure

The 5-mm sheets were successfully processed by laser-MIG hybrid welding, and no porosity or defects were observed; in comparison to welds produced with the same laser power and arc parameter by laser beam and MIG arc welding, respectively. The images of typical weld beads are shown in Fig. 2. The hybrid welding bead surface was very smooth and regular. However, the penetration of MIG arc welding bead was only about 1 mm, but the reinforcement was much higher than that of the hybrid welding joint. This outcome is attributed to the low welding current resulting in low heat input and melting capacity in MIG arc welding. Furthermore, given the unstable MIG arc, welding beadings defects were observed on the surface. For the laser welded bead, undercut was found due to the vaporization of the low boiling point alloying element (Li and Mg); rough weld bead surface was also observed. In the hybrid welding, the extra heat input from the arc enlarged the weld pool volume, which increased the laser power efficiency and resulted in the occurrence of the keyhole-welding mode. Furthermore, the laser power had an excellent effect on the stability of the MIG arc, which damped down the weld pool fluctuation and formed a smooth weld bead surface.

3.2 Microstructure and mechanical properties

The optical micrograph of the 1420 aluminum alloy is shown in Fig. 3. The base metal is characterized by a laminated structure. The elongated grains are formed in a pancake shape with their interfaces or grain boundaries parallel to the rolling plane [5]. Figure 4 shows the typical optical microstructure of the joint by hybrid welding. The

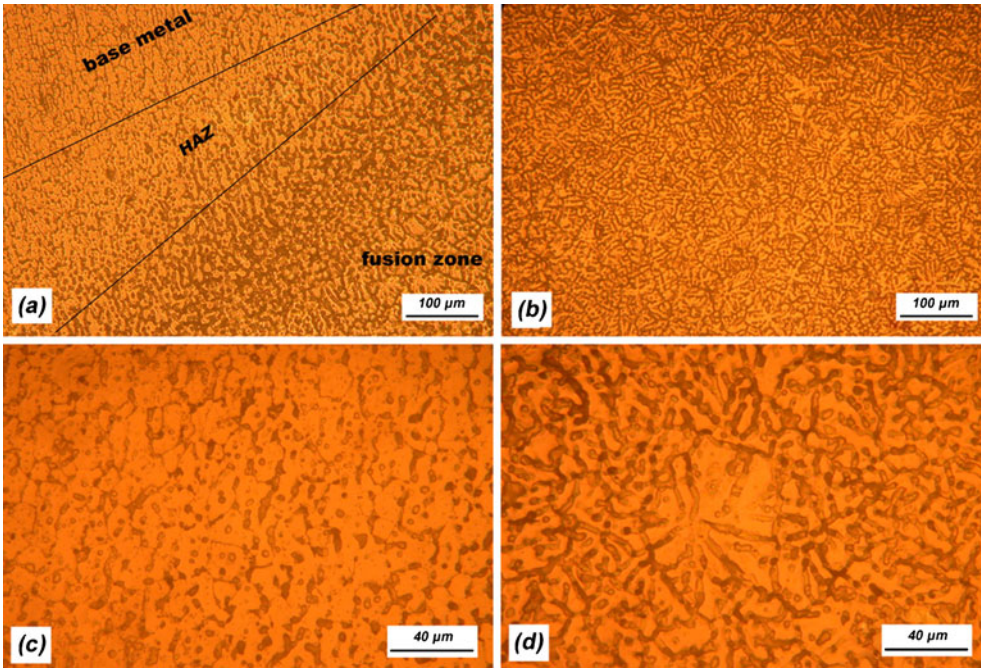

Fig. 4 Microstructure of joint. **a** Microstructure near the junction. **b** Network dendrites zone in the joint center. **c** HAZ with high magnification. **d** Network dendrites zone in the joint center with high magnification

base metal, HAZ, and fusion zone are clearly distinguished in Fig. 4a. The equiaxed grains are formed along the fusion boundary due to the high thermal gradient and small growth rate. Figure 4c, d present much higher magnification micrographs to show the morphology of the HAZ and fusion zone, respectively. The microstructure exists as a predominantly discontinuous equiaxed dendritic structure in the HAZ, and as a fine cellular dendritic structure in the fusion zone.

Standard heat treatment on the joint was performed using the procedures described above. The microstructure of the joint after solution heat treatments is shown in Fig. 5. Compared with the image in Fig. 4a, the microstructures changed from a dendritic structure to spheroidal grains. Figure 5a shows the differences in the grain size of the HAZ and fusion zone. The grain size of the HAZ is obviously larger than that of the base metal, whereas the fusion zone shows the largest grain size.

The transverse tensile strength of the parent material and the joints before and after heat treatment was evaluated. In each condition, three specimens were tested, and the average tensile strength of three results was obtained. For all the joints, failure occurred only in the weld metal region. The tensile strengths of the joints before and after heat treatment were 223 and 267 MPa, reaching up to 57 and 68 % of the parent materials' strength, respectively.

Microhardness tests were conducted on the transverse cross-sections of the samples. Results for the as-welded and heat treatment conditions are plotted in Fig. 6. The microhardness decreased over the fusion and HAZ in the as-welded samples. The average microhardness of the base metal was about Hv115, whereas the fusion was about Hv75. After the solution heat treatment and natural aging, the hardness recovered substantially to a level similar to that of the parent material in both the HAZ and fusion zone. The average microhardness was about Hv100.

The precipitate strengthened alloys show a decrease in the mechanical properties in the weld zone because of the dissolution and growth of the strengthening precipitates during the welding thermal cycle. A homogenization heat treatment of the welded samples is a logical solution to eliminate the alloying microsegregation and improve the

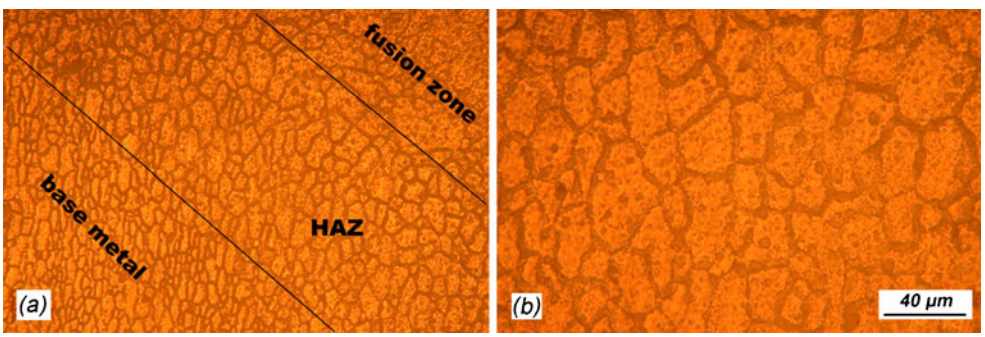

Fig. 5 Microstructure of joint after heat treatment. **a** Microstructure near the junction. **b** Microstructure in the joint center

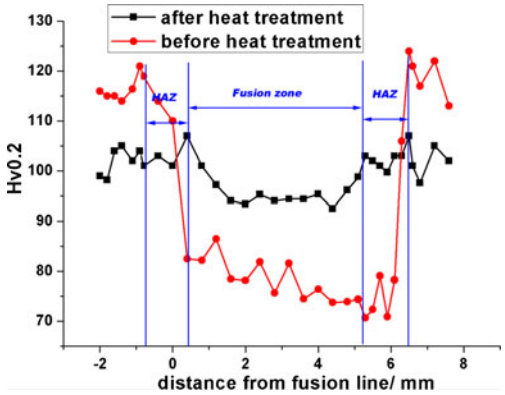

Fig. 6 Microhardness of joint before and after heat treatment

weld hardness. The prime precipitate of 1420 aluminum alloy is the δ′(Al_3Li) phase, and the formation and distribution of these precipitates depend on the solution treatment and aging treatment. The whole microstructure evolution process consists of three stages [18]. First, the primary dendritic grains coarsen into interconnected non-dendritic grains and recrystallization occurs. Second, the eutectics melt along the primary α-Al and the recrystallized grain boundaries, and the new recrystallized grains combine and grow. Finally, the grains become separated from each other and spheroidized at the heat treatment temperature range. In other words, the dendritic grains dissolve completely and the alloy elements distribute uniformly during the solution heat treatment. After the quenching treatment, a supersaturated solid solution is formed. The long exposure in air during the artificially aged process promotes the atom diffusion. Finally, particles of the δ′(Al_3Li) phase are very fine and seem to be uniformly distributed throughout the matrix. This outcome leads to an increase in dislocation density, which results in an improvement in hardness and enhanced tensile properties.

3.3 Fracture behavior

Figure 7 shows the SEM fractographs of the base metal. The fractographs are characterized by the appearance of the banding and delamination features, indicating an extensive shear-dominated planar slip. The laminated structure is shown more clearly in Fig. 7d. However, the fracture modes of the joints are different from that of the base metal. Figures 8 and 9 show the SEM fractographs of the joints as-welded condition and after heat treatment, respectively. Different fracture modes are clearly observed between the two joints. The fracture morphology of the joint as-welded condition exhibits the characteristics of dominated dimples and a small amount tear ridges (shown in Fig. 8b), which are associated with the mixed ductile and brittle facture

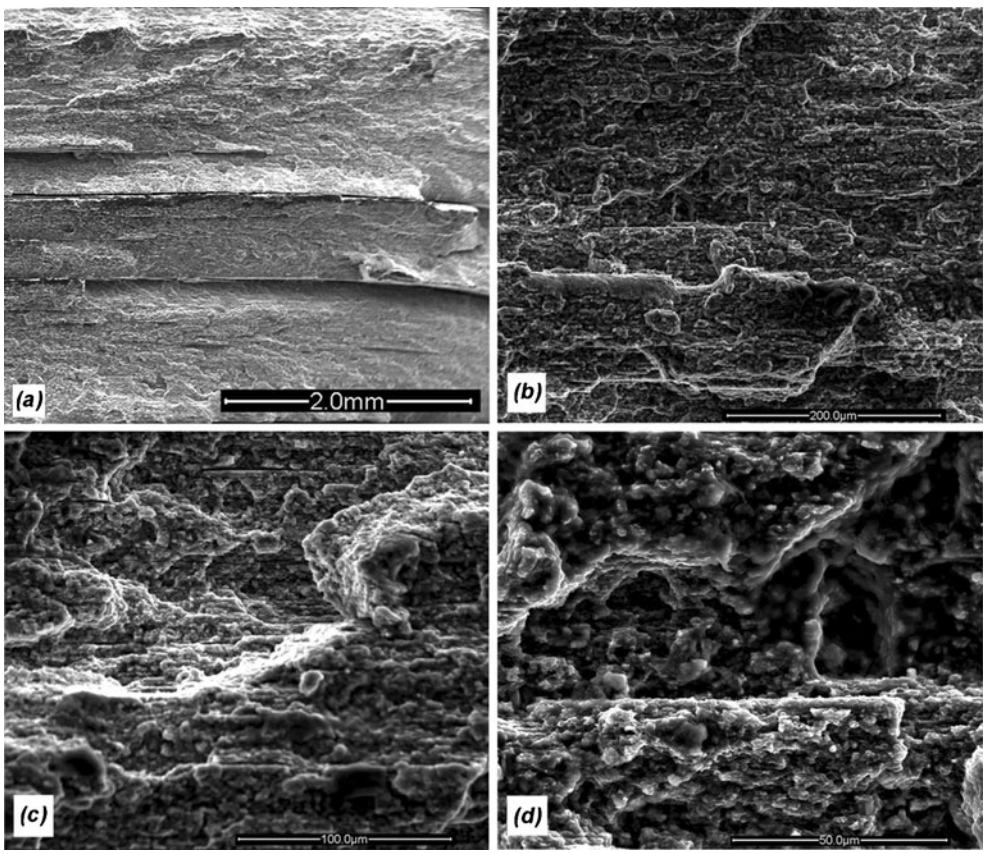

Fig. 7 SEM fractographs of base metal

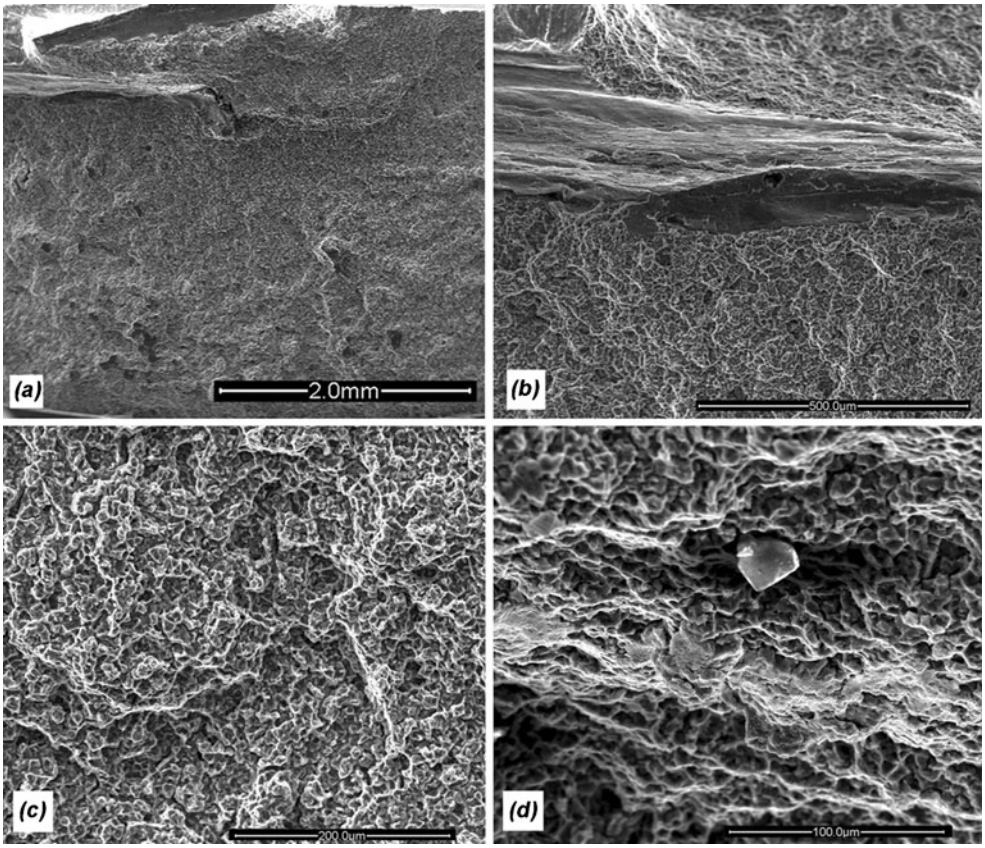

Fig. 8 SEM fractographs of joint as-welded condition

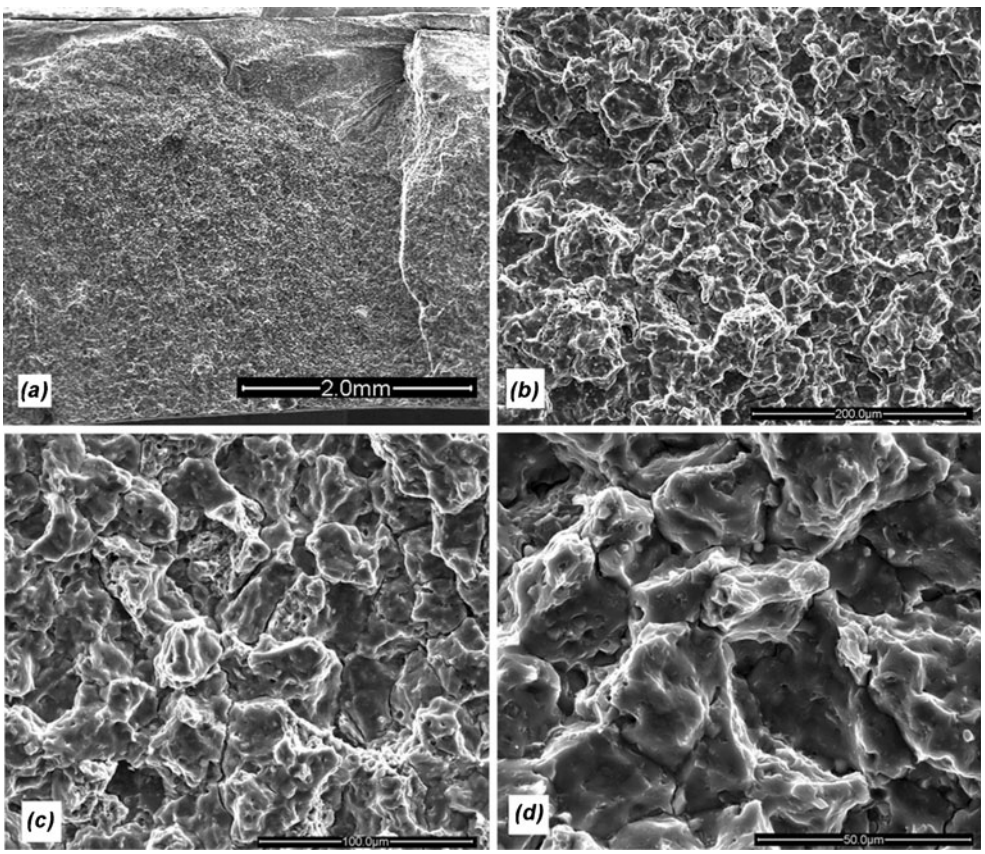

Fig. 9 SEM fractographs of joint after heat treatment

mechanisms. Coarse dimples and voids are observed in the joint [19]. The voids relate to isolated second phases on the dendrite boundaries, and the coarse dimples decrease the tensile strength and elongation. However, the macroscopic shear fracture is not observed, but the fracture surfaces are perpendicular to the tensile axis in the joint after heat treatment. Furthermore, the fracture mode transforms from a transgranular to an intergranular fracture [3]. The cleavage cracking coupled with an intergranular microvoid coalescence fracture mechanism occurs. Overall morphology at the higher magnifications is predominantly intergranular with a distinct absence of layered ledges or groove-like features [20].

4 Conclusions

The 5-mm-thick 1420 Al-Li alloy plates were welded by laser, MIG arc, and laser-MIG arc hybrid welding, respectively. Full penetration joints without any defects were produced by hybrid welding. The microstructure characteristics, mechanical properties, and fractographs of the hybrid welding joints in the as-welded condition and after heat treatment were investigated. The following conclusions are derived from the experimental results and discussion.

1. The microstructure of the HAZ exists as a predominantly discontinuous equiaxed dendritic structure, whereas that of the fusion zone exists as a fine cellular dendritic structure. After heat treatment, the microstructures change from a dendritic structure to a spheroidal crystal; the grain size of the HAZ is obviously larger than that of base metal, whereas the fusion zone shows the largest grain size.
2. The tensile strengths of joints before and after heat treatment were 223 and 267 MPa, reaching up to 57 and 68 % of the parent materials' strength, respectively. The microhardness decreases over the fusion zone and the HAZ in the as-welded condition. After heat treatment, the hardness recovers substantially to a level similar to that of the parent material.
3. The joint as-welded condition exhibits the characteristics of dominated dimples and a small amount tear ridges, which are associated with the mixed ductile and brittle facture mechanisms. The fracture mode transforms from a transgranular to an intergranular fracture after heat treatment; the cleavage cracking coupled with an intergranular microvoid coalescence fracture mechanism occurs.

Acknowledgments The authors gratefully acknowledge the financial support by Innovation Research Fund of Huazhong University of Science and Technology (no. 2011JC020).

References

1. Pickens JR (1985) Review: the weldability of lithium-containing aluminum alloys. J Mater Sci 20:4247–4258
2. Madhusudhan RG, Amol AG (1997) Weld microstructure refinement in a 1441 grade aluminium–lithium alloy. J Mater Sci 32:4117–4126
3. Chen SC, Huang JC (1999) Influence of welding parameters on microstructures and mechanical properties of electron beam welded aluminum–lithium plates. Mater Sci Tech-Lond 15 (8):965–978
4. Wei ST, Hao CY, Chen JC (2007) Study of friction stir welding of 1420 aluminum–lithium alloy. Mat Sci Eng A-Struct 452:170–177
5. Shi YW, Zhong F, Li XY, Gong SL, Chen L (2007) Effect of laser beam welding on tear toughness of a 1420 aluminum alloy thin sheet. Mat Sci Eng A-Struct 465:153–159
6. Padmanabham G, Pandey S, Schaper M (2005) Pulsed gas metal arc welding of Al-Cu-Li alloy. Sci Technol Weld Joi 10(1):67–74
7. Cavaliere P, Cabibbo M, Panella F, Squillace A (2009) 2198 Al-Li plates joined by friction stir welding: mechanical and microstructural behavior. Mater Design 30:3622–3631
8. Kanwer SA, Sunil P, Michael S, Rajneesh K (2010) Effect of process parameters on friction stir welding of aluminum alloy 2219-T87. Int J Adv Manuf Technol 50:941–952
9. Reinhold B (2006) Nd:YAG laser butt welding of AA6013 using silicon and magnesium containing filler powders. Mat Sci Eng A-Struct 426:250–262
10. Aalderinka BJ, Aarts RGKM, Lange DFD, Meijer J (2007) Experimental observation of keyhole shapes in the laser welding of aluminum blanks. J Laser Appl 19(4):245–251
11. Lee MF, Huang JC, Ho NJ (1996) Microstructural and mechanical characterization of Laser beam welding of a 8090 AI-Li thin sheet. J Mater Sci 35:1455–1468
12. Xu GX, Wu CS, Qin GL, Wang XY, Lin SY (2011) Adaptive volumetric heat source models for laser beam and laser + pulsed GMAW hybrid welding processes. Int J Adv Manuf Technol 57:245–255
13. Zhang DQ, Li J, Joo HG, Lee KY (2009) Corrosion properties of Nd:YAG laser-GMA hybrid welded AA6061 Al alloy and its microstructure. Corros Sci 51(6):1399–1404
14. Kim YP, Alam N, Bang HS, Bang HS (2006) Observation of hybrid (cw Nd:YAG laser MIG) welding phenomenon in AA 5083 butt joints with different gap condition. Sci Technol Weld Joi 11(3):295–307
15. Campana G, Ascari A, Fortunato A, Tani G (2009) Hybrid laser-MIG welding of aluminum alloys: the influence of shielding gases. Appl Surf Sci 255:5588–5590
16. Tong H, Ueyama T, Nakata K, Ushio M (2003) High speed welding of aluminum alloy sheets using laser assisted alternating current pulsed metal inert gas process. Sci Technol Weld Joi 8(3):229–234
17. Casalino G (2007) Statistical analysis of MIG-laser CO_2 hybrid welding of Al-Mg alloy. J Mater Process Tech 191:106–110
18. Wang JG, Lu P, Wang HY, Liu JF, Jiang QC (2005) Semisolid microstructure evolution of the predeformed AZ91D alloy during heat treatment. J Alloys Compd 395:108–112
19. Lakshminarayanan AK, Balasubramanian V, Elangovan K (2009) Effect of welding processes on tensile properties of AA6061aluminium alloy joints. Int J Adv Manuf Technol 40:286–296
20. Balasubramanian V, Ravisankar V, Madhusudhan Reddy G (2008) Effect of pulsed current welding on mechanical properties of high strength aluminum alloy. Int J Adv Manuf Technol 36:254–262